

# Analysis and Design of a High Voltage Flyback Converter with Resonant Elements

Sung-Soo Hong\*, Sang-Keun Ji\*, Young-Jin Jung\*, and Chung-Wook Roh†

†\* Dept. of Electrical Engineering, Kookmin University, Seoul, Korea

## Abstract

This paper presents the operational characteristics of a high voltage flyback converter with resonant elements. In high voltage low power applications, the effect of a transformer's stray capacitance might be the most important factor that influences the overall performance of the circuit. A detailed mode analysis and the design procedure are presented in designing the high voltage flyback converter. To verify and confirm the validities of the presented analysis and design procedure, a computer simulation and experiments have been performed.

**Key Words:** Flyback converter, High voltage power supply, Resonant elements, Stray capacitance

## I. INTRODUCTION

Flyback converters have been widely used because of their relative simplicity and their excellent performance for multi-output applications. They can save cost and volume compared with the other converters, especially in low power applications.

In a flyback converter, a transformer is adopted to achieve galvanic isolation and energy storage. Research is mainly focused on the leakage inductance of the transformer [1]–[3], since voltage spikes caused by the series resonance between the transformer leakage inductance and the parasitic capacitance of the switch are the dominant factors in determining the power conversion efficiency and the switching noise in low output voltage and high output current applications.

On the other hand, in high output voltage and low output current applications such as the high output voltage power supply (HVPS) in printers, the horizontal deflection circuit in cathode-ray tubes (CRT) displays, etc., the aforementioned resonance is not the main factor which degrades the performance of a flyback converter. Instead, the parallel resonance between the transformer's magnetizing inductance and the parasitic capacitance of the transformer are the dominant factors, since the large number of turns of the secondary windings generate a large parasitic capacitance.

The duty cycle loss due to this resonance is a severe problem in such high output voltage applications. Beside the problem of low power conversion efficiency, the expected output voltage in the kilo voltage range cannot be obtained in the first prototype based on the conventional design method. A redesign of the transformer based on the trial and error process is inevitable in this case. This results in a lengthy

process for developing a high output voltage flyback converter [4]–[6]. Therefore, it is very important for the optimum design of a high voltage flyback converter to take into consideration the resonance between the magnetizing inductance and the parasitic capacitance of the high voltage transformer which has large secondary winding turns [7], [8]. In this paper, the operational characteristics and an analysis considering the resonance effect is provided in details. A design example of a high voltage flyback converter with resonant elements is also presented. Finally, an experimental prototype circuit with an output of 1200V is provided to demonstrate the performance characteristics and design procedure of a high voltage flyback converter with resonant elements.

## II. THE OPERATIONAL CHARACTERISTICS

### A. Circuit Configuration

Fig. 1 shows the flyback converter with a high voltage flyback transformer, having high turns ratio between the primary and secondary windings considered in this paper. This flyback converter with resonant elements is composed of resonant tank networks including the parasitic capacitor of the switch ( $C_p$ ), the transformer magnetizing inductance ( $L_m$ ), the parasitic capacitor of the diode ( $C_s$ ) and the winding capacitance ( $C_{ws}$ ). Since the capacitance on the secondary side is reflected to the primary side with the value of  $n^2$  times, where  $n$  is the turn ratio of the transformer and the winding capacitance ( $C_{ws}$ ) is sufficiently large compared with that of a conventional transformer. Thus, the resonance between the parasitic capacitance  $C_{ws}$  and the magnetizing inductance which arise during the turn-on and turn-off transitions of the semiconductor elements is the dominant factor which affect the duty cycle loss [9].

This circuit can be transformed to an equivalent circuit on the primary side, as shown in Fig. 2. A process to determine

Manuscript received Nov. 4, 2009; revised Jan. 6, 2010

† Corresponding Author: drno@kookmin.ac.kr

Tel: +82-2-910-4947, Fax: +82-2-910-4449, Kookmin University

\*Dept. of Electrical Engineering, Kookmin University, Korea

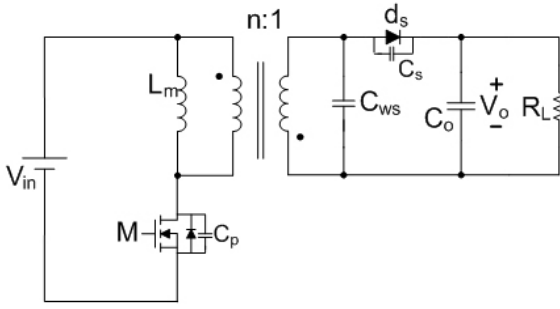


Fig. 1. Flyback Converter with Resonant Elements.

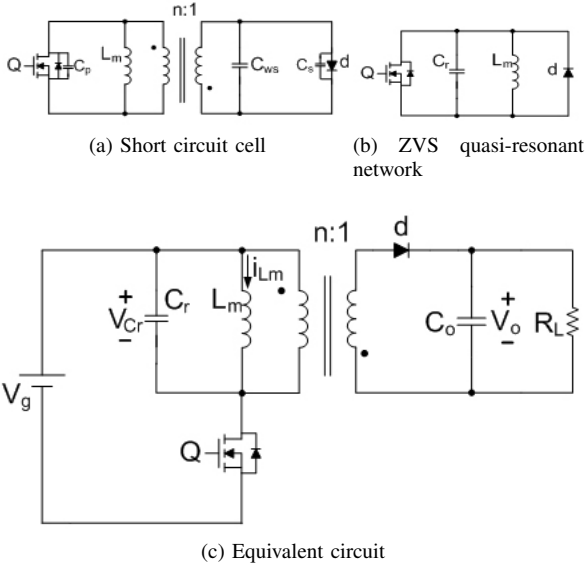


Fig. 2. Equivalent Circuit of high voltage Flyback Converter with Resonant Elements.

the topology of a resonant switch network is to replace all the low-frequency filter inductors with open circuits, and to replace all the dc sources and low-frequency filter capacitors with short circuits [10]. The elements of the resonant switch cell remain in Fig. 2(a). The parasitic capacitance of the diode ( $C_s$ ) and the winding capacitance ( $C_{ws}$ ) on the secondary side are reflected to the primary side with the value of  $n^2$  times. In the case of the zero-voltage-switching (ZVS) quasi-resonant switch, the network of Fig. 2(b) is always obtained, where the parasitic capacitances referred to the primary side are given as follows:

$$C_r = C_p // \frac{C_{ws}}{n^2} // \frac{C_s}{n^2}. \quad (1)$$

So this simplified flyback equivalent circuit which consists of magnetizing inductance ( $L_m$ ) and stray capacitance ( $C_r$ ) is shown in Fig. 2(c).

### B. Operational Principles

For the convenience of the mode analysis in the steady state, several assumptions are made as follows:

- The semiconductor devices are ideal, i.e., there is no forward voltage drop in the on-state, no leakage current in the off-state, and no time delay at both turn-on and turn-off.

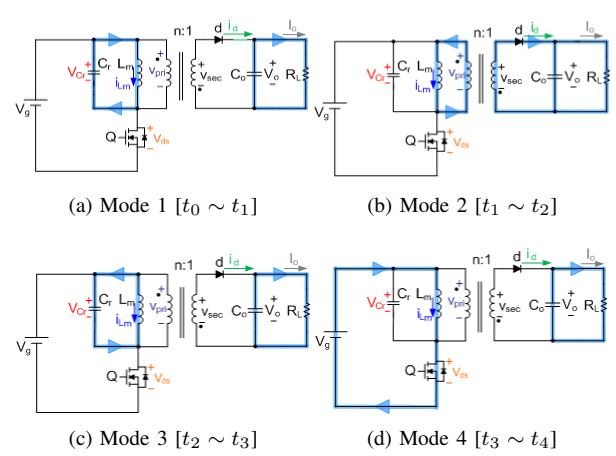


Fig. 3. Four operating modes of high voltage flyback converter with resonant elements.

- The converter is operated in the boundary conduction mode (BCM) [11], [12].
- The output capacitors  $C_o$  is sufficiently large. Therefore the output voltage can be assumed to be a constant DC voltage during the switching period  $T_s$ .
- The following variables are defined as follows:
  - Characteristic impedance  $Z_o = \sqrt{L_m/C_r}$ .
  - Resonant frequency  $f_o = 1/2\pi\sqrt{L_m C_r}$ .
  - Characteristic impedance ratio  $Q_p = \sqrt{n^2 R_L/Z_o}$ .
  - Normalized switching frequency ratio  $f_{ns} = f_s/f_o$ , where  $f_s$  is the switching frequency of the converter.

The steady-state voltage and current waveforms for each operating mode of the circuit shown in Fig. 2(c) are illustrated in Fig. 3. There are four stages during one switching period. The corresponding key waveforms are given in Fig. 4. Every cycle of the converter's operation can be divided into the following intervals, depicted in Fig. 4: ( $t_0, t_1$ ), the resonance of  $L_m$  and  $C_r$ ; ( $t_1, t_2$ ), the linear discharging of  $L_m$ ; ( $t_2, t_3$ ), the resonance of  $L_m$  and  $C_r$ ; ( $t_3, t_4$ ), the conduction of  $Q$ .

#### Mode 1 [ $t_0 \sim t_1$ ]: Resonant Interval

Prior to  $t_0$ , the switch  $Q$  is conducting and  $V_g$  is applied to the primary winding. When  $Q$  is turned off at  $t=t_0$ , the former operational mode, where the magnetizing current  $i_{Lm}$  is linearly ramped up, ends. Because of the resonance between  $L_m$  and  $C_r$ , the magnetizing energy in  $L_m$  is not immediately transferred to the secondary side. The energy transfer to the secondary side is delayed until the parasitic capacitor  $C_r$  is charged to  $V_{Cr}(t) = -nV_o \cdot V_{dc}$ .  $V_{dc}$  increases from 0 to  $V_g + nV_o$ . In mode 1, the current and voltage can be represented as follows:

$$v_{Cr}(t) = V_g \cos \omega_0 t - \tilde{i}(0) Z_o \sin \omega_0 t \quad (2)$$

$$i_{Lm}(t) = \frac{V_g}{Z_o} \sin \omega_0 t + \tilde{i}(0) \cos \omega_0 t \quad (3)$$

where  $\omega_o = 1/\sqrt{L_m C_r}$ ,  $Z_o = \omega_o L_m$ .

This mode ends when  $V_{Cr}(t) = -nV_o$  at  $t=t_1$ . At  $t=t_1$ , the diode  $D$  on the secondary side is turned on. From equation (2), the stray capacitance voltage  $V_{Cr}(t_1)$  can be obtained as:

$$-nV_o = V_g \cos \theta_1 - \tilde{i}(0) Z_o \sin \theta_1 \quad (4)$$

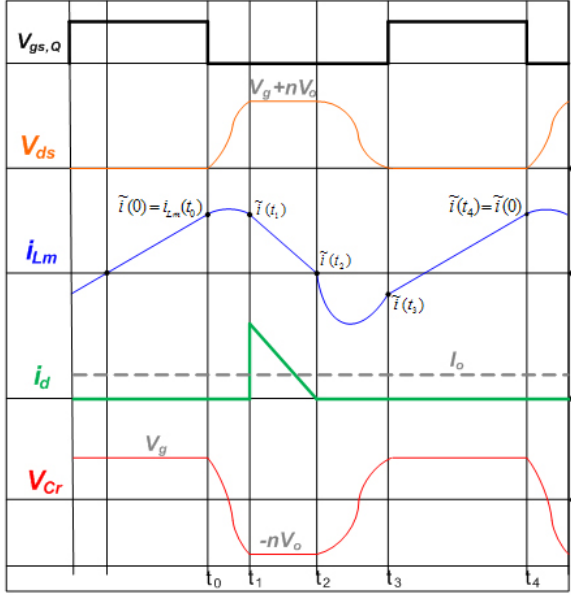


Fig. 4. Key waveforms of high voltage flyback converter with resonant elements.

where  $\theta_n = \omega_0(t_n - t_{n-1})$ . Hence,  $\theta_1 = \omega_0(t_1 - t_0)$ .

The switch conversion ratio  $M$  reflected to the primary side is given by  $nV_o/V_g$  and can be represented as follows:

$$M + \cos \theta_1 - \frac{\tilde{i}(0)Z_o}{V_g} \sin \theta_1 = 0. \quad (5)$$

#### Mode 2 [ $t_1 \sim t_2$ ]: Discharging Interval

When  $V_{Cr}(t)$  reaches  $-nV_o$  at time  $t=t_1$ , the diode in the secondary side is turned on and the magnetizing current in  $L_m$  flows to the secondary side. The magnetizing inductor current  $i_{Lm}$ , flowing through the path  $L_m - d - C_o$ , is expressed as:

$$i_{Lm}(t) = -\frac{nV_o}{L_m}(t - t_1) + \tilde{i}(t_1). \quad (6)$$

It is noted that  $V_{Cr}$  remains at  $-nV_o$ . The voltage across the primary switch is given during this mode by  $V_{dc} = V_g + nV_o$  which is the same as that of an ideal flyback converter. The energy stored in the primary inductance of the transformer is transferred to the load. At  $t=t_2$ , the stored energy is completely transferred, and  $\tilde{i}(t_2)$  becomes zero.

This state can be approximately described by the following equation:

$$-\frac{nV_o}{L_m}(t - t_1) + \tilde{i}(t_1) = 0 \rightarrow \theta_2 = \frac{Z_o \tilde{i}(t_1)}{nV_o}. \quad (7)$$

Substituting (7) into (3) leads to

$$\theta_2 M = \sin \theta_1 + \frac{\tilde{i}(0)Z_o}{V_g} \cos \theta_1. \quad (8)$$

#### Mode 3 [ $t_2 \sim t_3$ ]: Resonant Interval

After the energy stored in  $L_m$  is completely transferred to the output capacitor and the load on the secondary side, resonant occurs between  $C_r$  and  $L_m$ . When the current in  $L_m$  is zero, the diode on the secondary side is turned off.

However, the drain-source voltage of the switch  $V_{dc}$  does not immediately go to zero but a quasi resonant occurs. The resonant action of  $L_m$  and  $C_r$  causes  $V_{dc}$  to decrease to zero at  $t_3$ . Therefore the body diode of switch  $Q$  is turned on and it ensures the zero voltage switching (ZVS) operation. The inductor current  $i_{Lm}$ , flowing through the path  $L_m - d - C_o$ , is negative. The resonant voltage  $V_{Cr}$  and the resonant current  $i_{Lr}$  on the primary side can be expressed as:

$$v_{Cr}(t) = -nV_o \cos \omega_o t \quad (9)$$

$$i_{Lm}(t) = -\frac{nV_o}{Z_o} \sin \omega_o t. \quad (10)$$

This stage ends when  $V_{Cr}(t)$  reaches  $V_g$  at  $t=t_3$  and the following equations can be obtained from equation (9):

$$\cos \theta_3 = -\frac{1}{M}. \quad (11)$$

From the equation (11), it can be seen that the switch conversion ratio  $M$  should be at least larger than 1. The switch  $Q$  can operate with ZVS for  $M > 1$ .

#### Mode 4 [ $t_3 \sim t_4$ ]: Charging Interval

In this mode the switch  $Q$  is turned on and  $V_{dc}=0$ . Before the polarity of the current  $i_{Lm}$  changes, the main switch should be turned on to ensure ZVS operation. The input energy is stored in the magnetizing inductance  $L_m$ , via the path  $V_g - L_m - Q$ . The voltage  $V_{Cr}(t)$  remains  $V_g$ . The primary side current  $i_{Lm}$  increases linearly, and is expressed as:

$$i_{Lm}(t) = \frac{V_g}{L_m}(t - t_3) + \tilde{i}(t_3). \quad (12)$$

This mode ends when the switch  $Q$  is turned off. Since  $\tilde{i}(t_4) = \tilde{i}(0)$ , equation (12) can be written as:

$$\tilde{i}(0) = \frac{V_g}{Z_o} [\theta_4 - M \sin \theta_3]. \quad (13)$$

The output current  $I_o$  can be found by averaging the output diode current  $i_d(t)$  over one switching period as:

$$I_o = \frac{1}{T_S} \int_0^{t_4} i_d(t) dt = \frac{\theta_2}{\theta} \frac{\tilde{i}(t_1)}{2} \quad (14)$$

where  $\theta = \omega_o T_S$ . Substitution of (14) into (7) leads to:

$$\theta_2^2 = \frac{2\theta}{Q_p} \quad (15)$$

where  $Q_p = \frac{n^2 V_o}{Z_o I_o}$ . Combining (5) and (8) gives:

$$\theta_2 \sin \theta_1 = \cos \theta_1 + \frac{1}{M}. \quad (16)$$

Substitution of (5) into (13) leads to:

$$\frac{\cos \theta_1 + M}{\sin \theta_1} = -M \sin \theta_3 + \theta_4. \quad (17)$$

Based on (11), and (15)~(17) the expressions can be obtained as:

$$\theta_3 = \cos^{-1} \left( -\frac{1}{M} \right) \quad (18a)$$

$$\theta_2 = \sqrt{\frac{2\theta}{Q_p}} \quad (18b)$$

$$\theta_1 = \cos^{-1} \frac{-\frac{1}{M} + \theta_2 \sqrt{\theta_2 + 1 - \frac{1}{M^2}}}{\theta_2^2 + 1} \quad (18c)$$

$$\theta = \theta_1 + \theta_2 + \theta_3 + \theta_4 \quad (18d)$$

$$\theta_4 = \frac{\cos \theta_1 + M}{\sin \theta_1} + M \sin \theta_3. \quad (18e)$$

Expressions (18a)-(18e) will be used later to design the ZVS high voltage flyback converter with resonant elements.

### C. Voltage Conversion Ratio

The magnetizing current  $i_{Lm}$  during the entire mode of operation is expressed as:

$$\tilde{i}(t_1) = \frac{V_g}{Z_o} \sin \theta_1 + \tilde{i}(0) \cos \theta_1 \quad (19a)$$

$$\tilde{i}(t_2) = 0 = -\frac{nV_o}{Z_o} \theta_2 + \tilde{i}(t_1) \quad (19b)$$

$$\tilde{i}(t_3) = -\frac{nV_o}{Z_o} \sin \theta_3 \quad (19c)$$

$$\tilde{i}(t_4) = \tilde{i}(0) = \frac{V_g}{Z_o} \theta_4 + \tilde{i}(t_3). \quad (19d)$$

From (19b), the magnetizing current at  $t=t_1$  can be expressed as:

$$\tilde{i}(t_1) = \frac{nV_o}{Z_o} \theta_2. \quad (20)$$

Substitution of (20) into (19a) leads to:

$$\tilde{i}(0) = \frac{\frac{nV_o}{Z_o} \theta_2 - \frac{V_g}{Z_o} \sin \theta_1}{\cos \theta_1}. \quad (21)$$

From (21), (19d) can be expressed as:

$$\tilde{i}(t_3) = \frac{\frac{nV_o}{Z_o} \theta_2 - \frac{V_g}{Z_o} \sin \theta_1}{\cos \theta_1} - \frac{V_g}{Z_o} \theta_4. \quad (22)$$

The voltage conversion ratio can be calculated from the substitution of (22) into (19c) as follows:

$$\begin{aligned} \frac{V_o}{V_g} &= \frac{1}{n} \frac{\theta_4 \cos \theta_1 + \sin \theta_1}{\theta_2 + \cos \theta_1 \sin \theta_3} \\ &= \frac{1}{n} \frac{(t_4 - t_3) \cos \frac{(t_1 - t_0)}{\sqrt{L_m C_r}} + \sqrt{L_m C_r} \sin \frac{(t_1 - t_0)}{\sqrt{L_m C_r}}}{(t_2 - t_1) + \sqrt{L_m C_r} \cos \frac{(t_1 - t_0)}{\sqrt{L_m C_r}} \sin \frac{(t_3 - t_2)}{\sqrt{L_m C_r}}}. \end{aligned} \quad (23)$$

It is noted that if the time intervals at mode 1 and mode 3 are short, the voltage conversion ratio of equation (23) becomes as:

$$\frac{V_o}{V_g} = \frac{1}{n} \frac{(t_4 - t_3)}{(t_2 - t_1)} = \frac{1}{n} \frac{D}{1 - D} \quad (24)$$

where  $D$  is the duty cycle,  $D = t_4 - t_3$  and  $1 - D = t_2 - t_1$ . It is also noted that equation (24) is the same as the voltage conversion ratio of a conventional flyback converter.

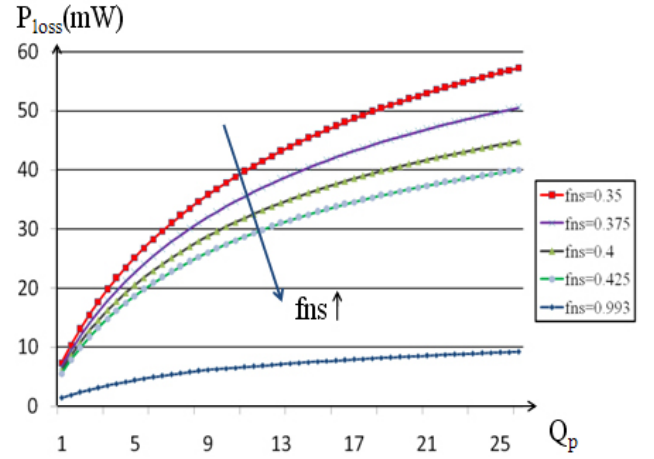


Fig. 5. Waveforms for the switch power loss as a function of  $Q_p$  and  $f_{ns}$ .

## III. DESIGN CONSIDERATIONS

### A. Switch Power Losses

The characteristic impedance ratio  $Q_p$  and the normalized switching frequency ratio  $f_{ns}$  are the most important parameters for a high voltage flyback converter with resonant elements because they determine the power loss. Since the load current is small in low power level high output voltage applications, the power loss of the switch is the dominant factor. For example, in a HVPS in a laser jet printer, whose power level is about 1Watt with an output voltage of 1,500 volt, the size and volume of the converter is determined mainly by the switch due to its large sized heatsink element.

The energy dissipated by the switch during the resonant periods, such as Mode 1 and Mode 3, is given by the current though the parasitic capacitance of the switch  $C_p$  multiplied by the drain-source voltage  $V_{ds}$ . During these resonant periods, the drain-source voltage of the switch  $V_{dc}$  can be expressed as:

$$\begin{cases} \text{Mode 1 : } v_{ds}(t) = V_g(1 - \cos \theta) + \tilde{i}(0)Z_o \sin \theta \\ \text{Mode 3 : } v_{ds}(t) = V_g + nV_o \cos \theta \end{cases} \quad (25)$$

The power loss of the switch during the resonant period is defined as an integral of the drain-source voltage of the switch multiplied by magnetizing inductance current and divided by the period  $T$ . In addition, because the magnetizing inductance current divides into the parasitic capacitance  $C_p$  and the resonant capacitance  $C_r$ , the impedance ratio should be multiplied. The power loss of the switch,  $P_{sw\_loss}$ , can be obtained as follows:

$$P_{sw\_loss} = \left[ \frac{V_g^2}{Z_o^2} (-\cos \theta_1 + 1) + V_g \tilde{i}(0) \sin \theta_1 + \frac{1}{2} \left( \tilde{i}(0)^2 Z_o - \frac{V_g^2}{Z_o} \right) \sin^2 \theta_1 - \frac{V_g \tilde{i}(0)}{2} \sin^2 \theta_1 \right] \times \frac{1}{\theta} \times \frac{C_p}{C_r} + \left[ \frac{nV_o}{Z_o} \left| V_g \cos \theta_3 - V_g - \frac{nV_o}{2} \sin^2 \theta_3 \right| \right] \quad (26)$$

The characteristics of the switch power loss during the resonant period are depicted in Fig. 5. These characteristics describes how, at a given  $f_{ns}$ , the power loss magnitude varies with the characteristic impedance ratio  $Q_p$ . We can minimize the power loss of the switch by optimal choices of  $Q_p$  and  $f_{ns}$ . The power loss decreases as  $Q_p$  decreases and  $f_{ns}$  increases. However, the switch conversion ratio  $M$  is less than 1 as  $Q_p$

decreases and  $f_{ns}$  increases. Therefore to obtain the minimum power loss of the switch  $Q_p$ , it is recommended to select a low value of  $f_{ns}$  and a high value of  $M$ , which determines the turns ratio of the transformer.

### B. Boundary Condition of the Resonant Capacitor

When designing a high voltage flyback converter with resonant elements, there exist a minimum value of the resonant capacitor  $C_r$ . The parasitic capacitances of the switch and diode are obtained from the available datasheet. There also exists a minimum winding capacitance on the large number of turns of the secondary windings. The parasitic capacitance of the diode ( $C_s$ ) and the winding capacitance ( $C_{ws}$ ) on the secondary side are reflected to the primary side with the value of  $n^2$  times. When selecting  $Q_p$  and  $f_{ns}$  it should be noted that there exists a minimum resonant capacitance  $C_r$ .

## IV. DESIGN PROCEDURE

From the operational analysis described above, the design process of a high voltage flyback converter with resonant elements is considered in this section and a design example is given based on a 150mW prototype converter.

**Step 1** Define the system specifications: The input voltage  $V_{in}$ , output voltage  $V_o$ , output power  $P_o$ , switching frequency  $f_s$ , parasitic capacitance of the switch  $C_p$ , parasitic capacitance of the diode  $C_s$  and the winding capacitance  $C_{ws}$ .

**Step 2** Select the characteristic impedance ratio  $Q_p$  and the normalized switching frequency ratio  $f_{ns}$ : The key design parameter is the power loss of the switch. Mechanisms that cause power loss are discussed in Chapter 3, including switching loss.

**Step 3** Determine  $M$  and  $\theta_1 \sim \theta_4$ : With  $Q_p$  and  $f_{ns}$  selected, the switch conversion ratio  $M$  is reflected to the primary side and the phase variables of each mode  $\theta_1 \sim \theta_4$  can be found from (18a~e). If  $M < 1$ , other values of  $Q_p$  and  $f_{ns}$  should be selected.

**Step 4** Determine the turns ratio  $n$  and the resonant elements such as  $L_m$  and  $C_r$ : The turns ratio  $n$  of the high voltage transformer can be found from  $M$  specified in Step 3.

$$n = M \frac{V_g}{V_o}. \quad (27)$$

The characteristic impedance  $Z_o$  and the resonant frequency  $f_o$  can be determined, using  $Q_p$ ,  $f_{ns}$  and equation (27).

$$Z_o = \frac{n^2 R_L}{Q_p}, \quad f_o = \frac{f_s}{f_{ns}}. \quad (28)$$

From equation (28), the resonant elements are obtained as:

$$L_m = \frac{Z_o}{2\pi f_o}, \quad C_r = \frac{1}{2\pi Z_o f_o}. \quad (29)$$

Check to see if the resonant capacitor  $C_r$  is larger than  $C_{r\min}$  equals  $C_s + C_{ws}$ . If not, return to Step 2, i.e. select other values of  $Q_p$  and  $f_{ns}$ .

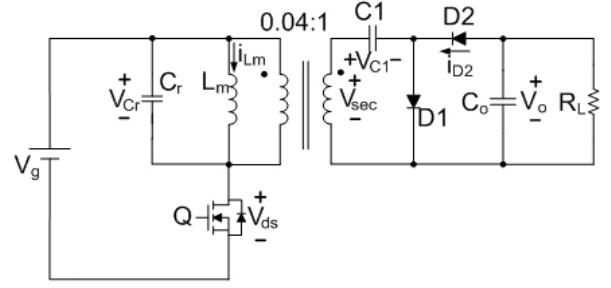


Fig. 6. Circuit topology design for high output voltage application :  $V_g = 24V$ ,  $V_o = -1220V$ ,  $V_{c1} = 610V$ ,  $Q = KSD526 - Y$ ,  $D1$ ,  $D2 = 718$ ,  $L_m = 100.8\mu H$ ,  $C_r = 50.58nF$ ,  $C_o$ ,  $C_1 = 470pF$ ,  $R_L = 10M\Omega$ .

**Step 5** Determine the maximum voltage and current stress on the switch: From equation (3), the peak current of the magnetizing inductance can be expressed as:

$$i_{Lm,pk} = \sqrt{\left(\frac{V_g}{Z_o}\right)^2 + (\tilde{i}(0))^2}. \quad (30)$$

The voltage stress of the switch and the output diode are expressed as:

$$V_{ds,max} = V_g + nV_o, \quad V_{d,max} = V_o + \frac{1}{n}V_g. \quad (31)$$

### A. Design Example

Low input voltage, high output voltage and low power level applications, are the areas where high voltage flyback converters can be particularly advantageous. As an example, we consider the design of a 150mW flyback DC-to-DC converter according to the following specifications:

- range of input voltage:  $V_{g,min}=24V$ ,  $V_{g,max}=27V$
- output voltage:  $V_o=-1.22kV$  (using voltage doubler:  $V_{c1}=610V$ )
- load range:  $12.2\mu A \leq I_o \leq 122\mu A$
- switching frequency:  $f_s=70kHz$
- minimum capacitance:  $C_p=90pF$ ,  $C_s=10pF$ ,  $C_{ws}=20pF$

The high output voltage flyback power circuit in this example is shown in Fig. 6. Using Step 2,  $Q_p$  and  $f_{ns}$  are selected as  $Q_p=84$  and  $f_{ns}=0.933$  respectively. It is noted that this design example features a low input voltage, an extremely high output voltage and a small load range in a real printer application. Thus,  $Q_p$  and  $f_{ns}$  are selected to be large values. From equation (19), the switch conversion ratio  $M$  and  $\theta_1 \sim \theta_4$  are obtained as  $M=1.0163$ ,  $\theta_1=2.362$ ,  $\theta_2=0.338$ ,  $\theta_3=3.321$  and  $\theta_4=0.253$  respectively. Since  $M > 1$ , we can proceed to the next step. From equation (27), the turns ratio  $n$  of the high voltage transformer is obtained as  $n=0.04$ . From equation (28), the characteristic impedance  $Z_o$  and the resonant frequency  $f_o$  are  $Z_o=44.66\Omega$  and  $f_o=70.45kHz$ . Finally, from equation (29), the resonant elements are obtained as  $L_m=100.8\mu H$  and  $C_r=50.58nF$ . We observe that  $C_r$  satisfies the desired constraint on the minimum  $C_r$ , where  $C_{r\min}=18.86nF$ . From (30), the peak current is  $i_{Lm,pk}=586mA$ . From (31), the peak drain-to-source and diode voltage are  $V_{ds,max}=48.4V$  and  $V_{d,max}=1210V$ , respectively. The key components include: the switch  $Q$ :  $KSD526-Y$  and the output diode  $D$ : 718.



## V. SIMULATION AND EXPERIMENT

To verify the analysis and design procedure presented in this paper a PSIM simulation and an experiment were carried out on an actual high voltage flyback converter with resonant elements using the specifications and parameters listed in Table 1. A schematic representation of the flyback converter modeled in the simulation program is shown in Fig. 6.

The high voltage flyback converter with resonant elements consists of an ideal transformer, a magnetizing inductance and a resonant capacitor. In order to make the design process more efficient, the PSIM simulation data contains key waveforms such as the voltage stress on the switch, the magnetizing inductor current and the resonant capacitor voltage. This flyback design example is included to demonstrate an application of the procedure, and the results are supported by a simulation. The simulation and theoretical results are compared in Table 2, which shows the design parameters and the simulated values of the key voltage and the current waveforms during the whole switching period. Fig. 7 shows the results of the PSIM simulation, which contains the key voltage and the current waveforms of the high voltage flyback converter. It can be seen that the PSIM simulation results coincide well with the predicted results shown in Fig. 4 and Table 2.

TABLE I  
PARAMETERS OF EXPERIMENTAL CIRCUIT

Part	Value	Type
Switch $Q$	$V_{ce} : 80V$	$KSD526-Y$
Diode ( $D_1, D_2$ )	$V_r : 6kV$	718
Transformer ( $L_m$ )	$100.8\mu H$	Ferrite Core
Capacitor ( $C_1, C_o$ )	$470pF$	$C_1$ : ceramics / $C_o$ : AL
Load Resistor ( $R_L$ )	$10M\Omega$	Non-Inductive Resistor

TABLE II  
DATA OF DESIGN VALUE AND IMULATION RESULT

Parameter	Design value	Simulation Result	Deviation
$V_c$	$-1220[V]$	$-1205[V]$	1.23[%]
$\tilde{i}(0)$	$233.2[mA]$	$218.3[mA]$	6.39[%]
$\tilde{i}(t_1)$	$211.0[mA]$	$210.1[mA]$	0.85[%]
$t_1 \sim t_0$	$5.338[\mu s]$	$5.35[\mu s]$	0.26[%]
$t_2 \sim t_1$	$0.877[\mu s]$	$0.89[\mu s]$	1.48[%]
$t_3 \sim t_2$	$7.502[\mu s]$	$7.49[\mu s]$	0.16[%]
$t_4 \sim t_3$	$0.571[\mu s]$	$0.56[\mu s]$	1.93[%]

TABLE III  
DATA OF MEASURED RESULT AND SIMULATION RESULT

Parameter	Measured result	Design result	Deviation
$V_o$	$-1226[V]$	$-1205[V]$	1.71[%]
$V_{ce,max}$	$50.3[V]$	$48.5[V]$	3.58[%]
$V_{cr,max}$	$24.7[V]$	$24.0[V]$	2.83[%]
$V_{cr,min}$	$-26.0[V]$	$-24.0[V]$	5.80[%]
$V_{sec,max}$	$637[V]$	$600[V]$	5.81[%]
$V_{sec,min}$	$-655[V]$	$-613[V]$	6.41[%]

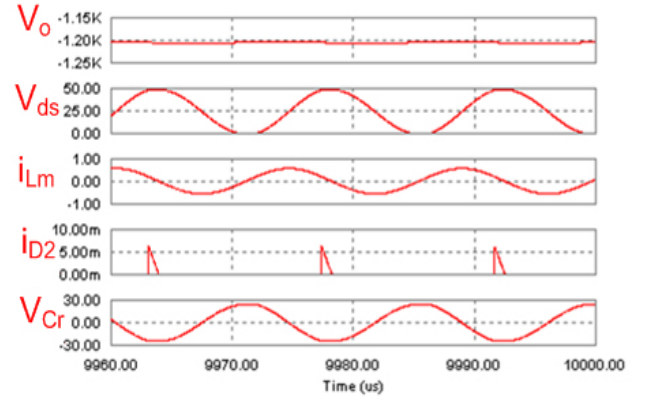
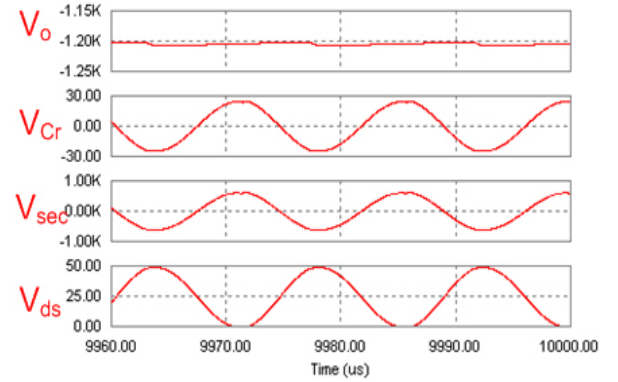
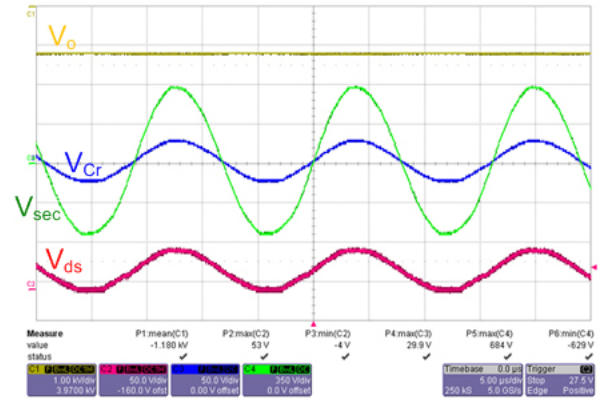


Fig. 7. PSIM simulation results for the design circuit operating at  $-1205V_{dc}$  output.



(a) Simulation results



(b) Experimental results

Fig. 8. Key waveforms of high voltage flyback converter.

Fig. 8 shows the experimental waveforms of Fig. 6,  $V_o$ ,  $V_{Cr}$ ,  $V_{sec}$  and  $V_{ds}$ , respectively. Each waveform shows good agreement with the simulation and the experimental results in TABLE III. As can be seen, the output voltage ( $V_o$ ) is about  $-1226V$ . The designed value and the simulated value are  $-1220V$  and  $-1205V$ , respectively. In addition, the measured output voltage was within 1.23% of the calculated value, verifying the accuracy of the equations given here. The other measured parameters are also similar to the calculated and simulated values.

The measured power loss of the switch is shown in Fig. 9 and TABLE IV, which shows the waveforms of  $V_{ce}$ ,  $I_c$

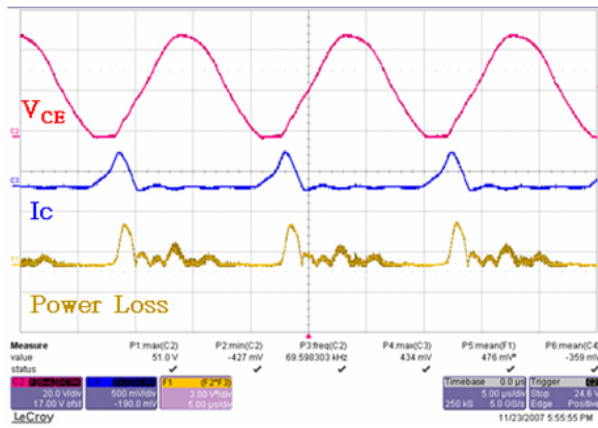


Fig. 9. Switch power loss of experimental measurements.

TABLE IV  
DATA OF MEASURED RESULT

Parameter	Measured result
$V_{ce,max}$	51.0[V]
$V_{ce,min}$	-0.4[V]
$I_{c,max}$	145[mA]
$P_{sw\_Loss}$	0.159[W]

and  $P_{sw\_Loss}$ , respectively. As can be seen, the power loss is negligible. The temperature of the switch is about 30.4°C at an ambient temperature of 24.1°C. It is verified that by considering the parasitic capacitance of transformer, the output voltage of the actual low power high voltage output flyback converter can be precisely predicted.

## VI. CONCLUSIONS

The effect of the resonant elements in a dc/dc converter with a transformer can be very important and must be considered when designing a high voltage flyback converter. The first requirement of a flyback converter used in low power level high output voltage applications is that the output voltage should be obtained at the expected value. Unlike an ideal flyback converter, the output voltage of a real converter is restricted by the parasitic properties of the high voltage flyback transformer. The influence of the transformer's stray capacitance is dominant.

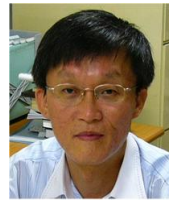
In this paper, to analyze the effects of these resonant elements, an equivalent circuit was derived. The design considerations and a design example of a high voltage flyback converter with 150mW have been presented. The design, simulation and experimental results were also given and the results agree well with the analytical results. This design procedure is expected to be well suitable for high output voltage applications.

## ACKNOWLEDGMENT

This work was supported by the research program 2010 of Kookmin University, Korea and also by the Ministry of Knowledge Economy (MKE), Korea, under the Information Technology Research Center (ITRC) support program supervised by the Institute of Information Technology Advancement (IITA) under Grant IITA-2009-C1090-0904-0002.

## REFERENCES

- [1] Shelton Gunewardena, Wendel E. Archer, Robert O. Sanchez, "High voltage miniature transformer design," *Electrical Insulation Conference and Electrical Manufacturing & Coil Winding Conference, 2001 Proceedings*, pp.141-147, 2001.
- [2] M. J. Prieto, A. Fernandez, J. M. Diaz, J. M. Lopera, J. Sebastian, "Influence of transformer parasitics in low-power applications," *Applied Power Electronics Conference and Exposition, 1999 APEC'99 Fourteenth Annual*, Vol.2, pp.1175-1180, Mar. 1999.
- [3] MIT, Staff of Dept of EE, *Magnetic circuit and transformer*, MIT Press, 1965
- [4] McArdle, J., Wilson, T.G. Jr., and Wong, R.C., "Effects of power-train parasitic capacitance on the dynamic performance of DC-to-DC converters operating in the discontinuous MMF mode," *IEEE Trans. on Power Electron.*, Vol. 2, No. 1, pp.2-19, Jan. 1987.
- [5] Lu, H.Y., Zhu, J.G., Ramsden, V.S., and Hui, S.Y.R., "Measurement and modeling of stray capacitance in high frequency transformer," *IEEE Power Electronics Specialist Conf. Rec.*, pp.763-768, Jun. 1999.
- [6] Lu, H.Y., Zhu, J.G., and Hui, S.Y.R., "Experimental determination of stray capacitances in high frequency transformers," *IEEE Trans. on Power Electron.*, Vol. 18, No. 5, pp.1105-1111, Jun. 2003.
- [7] S.-K. Chung, "Transient characteristics of high-voltage flyback transformer operating," *Applied IEE Proceedings Electric Power Applications*, Vol. 151, No. 5, pp.628-634, Sep. 2004.
- [8] Huang Kewei, Li Jie, Hu Xiaolin, Fan Ningjun, "Analysis and simulation of the influence of transformer parasitics to low power high voltage output flyback converter," *IEEE Industrial Electronics International Symposium*, pp. 305-310, Jun. 2008.
- [9] Ramsden, V.S., Lu, H.Y., and Zhu, J.G., "Dynamic circuit modeling of a high frequency transformer," *IEEE Power Electronics Specialist Conf. Rec.*, Vol. 2, pp.1479-14857, May 1998.
- [10] Robert W. Dragan M, *Fundamentals of Power Electronics*, Boulder Colorado, 2002.
- [11] Tabisz, W.A.; Gradzki, P.M.; Lee, F.C.Y., "Zero-voltage-switched quasi-resonant buck and flyback converters- experimental results," *IEEE Trans. on Power Electron.*, Vol. 4, No. 2, pp.194-204, Apr. 1989.
- [12] Vorperian, V., "Quasi-square-wave converters: topologies and analysis," *IEEE Trans. on Power Electron.*, Vol. 3, No. 2, pp. 183-191, Apr. 1988.



**Sung-Soo Hong** received his B.E. degree in Electrical Engineering from Seoul National University, Seoul, Korea, in 1980, and his M.S. and Ph.D. in Electrical and Electronics Engineering from the Korea Advanced Institute of Science and Technology, Seoul, Korea, in 1986 and 1992, respectively. From 1984 to 1998, he was an Electronics Engineer with Hyundai Electronics Company. In 1993, he was with the Virginia Polytechnic Institute and State University, Blacksburg, as a Research Scientist. Since 1999, he has been an Assistant Professor in the Electronics Engineering Department, Kookmin University, Seoul, Korea. His research interests are in the areas of modeling and control techniques for power converters, EMI analysis and reduction techniques for power electronics circuits.



**Sang-Keun Ji** was born in Seoul, Korea in 1981. He received his B.S. and M.S. in Electronics Engineering from Kookmin University, Seoul, Korea, in 2007 and 2009, respectively, where he is currently working toward his Ph.D. in the School of Electronics Engineering. His research interests are in the areas of high-efficiency power converters and renewable energy applications. Mr. Ji is a member of KPIPE (Korean Institute of Power Electronics).



**Young-Jin Jung** was born in Seoul, Korea in 1978. He received his B.S. in Electronics Engineering from Suwon University, Suwon, Korea, in 2004. He received his M.S. in Electronics Engineering from Kookmin University, Seoul, Korea, in 2008. Since 2006, he has been with Department of Power Electronics, Kookmin University, where he is currently a doctoral student. His research interests are in the areas of modeling and control of converters and inverters. Mr. Jung is a member of KPIPE (Korean Institute of Power Electronics).



**Chung-Wook Roh** was born in Korea in 1971. He received his B.S., M.S., and Ph.D. in Electrical Engineering and Computer Science from the Korea Advanced Institute of Science and Technology (KAIST), Taejeon, Korea, in 1993, 1995, and 2000, respectively. In 2000, he joined the Digital Media Network Division, Samsung Electronics Company, Suwon, Korea, where he was a Project Leader of the Plasma Display Driver Development Team. Since 2004, he has been with the department of Electrical Engineering, Kookmin University, Seoul, Korea where he is currently an Associate Professor. His research interests include driver circuits of displays such as light emitting diodes, plasma display panels,

low-power circuits for flat panel displays, as well as the modeling, design, and control of power conversion circuits, soft-switching power converters, resonant inverters, and electric drive systems. He is the author or coauthor of more than 100 technical papers published in journals and conference proceedings and has more than 50 patents. Dr. Roh has received several awards including a Best Presentation Award from the annual conference of the IEEE Industrial Electronics Society in 2002, a Best Paper Award from the Korean Institute of Power Electronics in 2003 and a Best Paper Award from the Korean Institute of Power Electronics in 2009, respectively. He is currently a journal editor for the Korean Institute of Power Electronics.